Manifestation of deformation and nonlocality in α and cluster decay

D. F. Rojas-Gamboa [*], J. E. Perez Velasquez,[†] and N. G. Kelkar [‡]

Departamento de Física, Universidad de Los Andes, Carrera 1 No. 18 A - 10, Bogotá 111711, Colombia

N. J. Upadhyay [§]

Department of Sciences, Amrita School of Engineering, Amrita Vishwa Vidyapeetham, Chennai 601103, India

It is common to study the strong decay of a heavy nucleus as a tunneling phenomenon where the α (^{4}He) or a light nuclear cluster tunnels through the Coulomb barrier formed by its interaction with the heavier daughter nucleus. The position and width of the Coulomb barrier is determined by the total interaction potential between the two daughter nuclei. We examine the effects of including nonlocality and deformation in the interaction potential by calculating the half-lives, $t_{1/2}$, and thereby phenomenological preformation factors of several nuclei, which have the possibility of decaying by emitting either an α or a light nuclear cluster. The effect of deformation manifests itself by a decrease in $t_{1/2}$ for all the decays studied. The effect of nonlocality is studied within two different models of the nuclear potential: the energy independent but angular momentum (l) dependent Mumbai (M) potential and the energy dependent Perey-Buck (PB) potential. The nonlocal nuclear interaction leads to a decrease in all half-lives studied. Though the decrease is larger due to the Perey-Buck potential, half-lives evaluated using the Mumbai potential show a strong sensitivity to the l value in the decay. This feature of the α and cluster decay half-lives can provide a complementary tool in addition to scattering data which are more commonly used to fix the parameters of a nonlocal potential in literature.

I. INTRODUCTION

α decay of radioactive nuclei, discovered in 1899 by Rutherford [1], is one of the most important decay modes in providing information about the structure of heavy nuclei such as the radius, deformation, and shell effects [2–4]. In addition to this, cluster radioactivity (CR) has also been very instrumental in providing structure information of heavy nuclei [5]. The spontaneous emission of light fragments heavier than the α particle but lighter than a typical mass of a light fragment in the fission process ($A \gtrsim 60$) is referred to as cluster radioactivity or cluster decay. Theoretically predicted cluster decay [6] was experimentally confirmed in 1984 by Rose and Jones [7]. Study of both the α and cluster decays for the isotopes of the same element provides insight about the impact of shell effects and deformations on the probabilities of these processes. In an investigation involving the comparison of different models for cluster radioactivity in superheavy nuclei [8], the authors found that a universal decay law which can predict light and heavy CR leads to the shortest half-lives when the daughter nuclei are around the doubly magic ^{208}Pb nucleus. Another interesting conclusion was that the CR dominates over α decay for $Z \geqslant 118$ nuclei. Because of the

large difference in the masses of the cluster and the daughter nucleus, just like the α decay, the cluster decay is also treated as a tunneling problem for the calculation of half-lives of nuclei.

In a recent work [9], we have investigated the effects of nonlocality on α-decay half-lives of nuclei. It is observed that the effective potential obtained between the α and the daughter nucleus within the nonlocal framework decreases the half-lives. This study was limited to α decay involving spherical nuclei and deformation was not considered. In the present work, we study the nonlocal effect for the α and cluster decay modes of a given parent nucleus. Furthermore, we also study the impact of nonlocality in the presence of deformation which modifies the barrier characteristics. In the α decay, the shape of the daughter nucleus contributes to the deformation term, whereas in the cluster decay, the shape of the lighter cluster in the decay channel contributes to the deformation.

The article is organized as follows. In Sec. II, we give a brief overview of the density-dependent double-folding (DF) model used to evaluate the potential between the cluster and the daughter nucleus followed by the formalism for the evaluation of decay half-lives. The two models used to study the nonlocal effects in the α and cluster decay of some heavy nuclei are also discussed. In order to extend the half-life calculations in the presence of deformation, we provide the details about the deformed DF nuclear potential and calculation of the half-lives from the deformed decay width. In Sec. III, we present the results and discuss them. Finally, in Sec. IV we summarize our findings.

———————
[*]df.rojas11@uniandes.edu.co
[†]je.perez43@uniandes.edu.co
[‡]nkelkar@uniandes.edu.co
[§]nupadhyay@mum.amity.edu

II. FORMALISM FOR α AND CLUSTER DECAY

In previous studies on α and cluster decay [2–4], it has been found that the half-life is an important observable related to the nuclear structure. In most of the theoretical models, the α and cluster decay half-life of a nucleus is evaluated as

$$t_{1/2} = \frac{\hbar \ln 2}{\Gamma}, \tag{1}$$

where the decay width Γ can be calculated within the framework of the semiclassical Jeffreys-Wentzel–Kramers–Brillouin (JWKB) approximation [10–12], as

$$\Gamma = P_i \frac{\hbar^2}{2\mu} \left[\int_{r_1}^{r_2} \frac{dr}{k(r)} \right]^{-1} \exp\left[-2 \int_{r_2}^{r_3} k(r) \, dr \right], \tag{2}$$

where $k(r) = \sqrt{\frac{2\mu}{\hbar^2} |V(r) - E|}$. P_i (with $i = \alpha$ or c) is the preformation factor in α or cluster (c) decay, μ is the reduced mass of the cluster-daughter system, and r_i ($i = 1, 2, 3$) are the three classical turning points. These latter are solutions of $V(r_i) = E$, where the energy E of the α particle or cluster is usually taken to be the same as the Q value for the decay. The exponential factor $\exp\left[-2 \int_{r_2}^{r_3} k(r) \, dr\right]$ is known as the penetration probability and the factor $[\int_{r_1}^{r_2} dr/k(r)]^{-1}$ in front of this arises from the normalization of the bound-state wave function in the region between the turning points r_1 and r_2 [10–12]. An essential ingredient for evaluating both factors is the interaction potential $V(r)$ between the emitted particle and the daughter nucleus that will be explained below. The appearance of a preformation factor P_i ($i = \alpha$ or c) in Eq. (2) takes into account the nonzero probability for the existence of the preformed cluster or α particle inside the parent as suggested by several theoretical models [13,14]. In the present study, we compare the effects of nonlocalities and deformation in different models. Hence, we shall set $P_i = 1$ when we compare the half-lives calculated within the different models.

A. Double folding model

α and cluster decay are treated as a tunneling problem where the emitted particle, preformed inside the parent nucleus, tunnels through the potential barrier. The interaction potential between the daughter nucleus and the cluster consists of the nuclear V_N, Coulomb V_C, and centrifugal potentials and is given by

$$V(r) = \lambda V_N(r) + V_C(r) + \frac{\hbar^2 \left(l + \frac{1}{2}\right)^2}{2\mu r^2}, \tag{3}$$

where r is the separation between the center of mass of the cluster and the center of mass of the daughter nucleus, l is the angular momentum carried by the emitted cluster, and λ is the strength of the nuclear interaction (see Fig. 1). The latter has been left as a parameter in order to ensure that the Bohr-Sommerfeld quantization condition [11] is satisfied. Thus λ fixes the strength of the nuclear potential. The centrifugal term containing, $l(l + 1)$, is replaced by the correction, $(l + \frac{1}{2})^2$, introduced by Langer when one uses the semiclassical approximation [15]. This is essential to ensure the correct behavior of
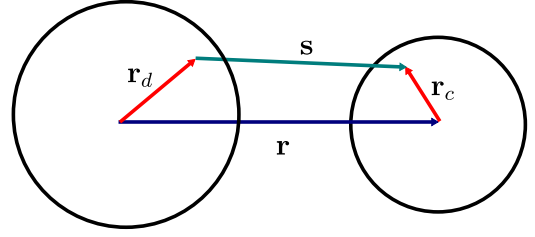

FIG. 1. Coordinates used in the DF calculations. Vectors $\mathbf{r}_c$ and $\mathbf{r}_d$ correspond to the position of a nucleon in the cluster and daughter nucleus, respectively.

the JWKB wave function near the origin. The potential used in the calculation then has three turning points, r_1, r_2, and r_3.

For the nuclear potential, it is desirable to relate the nucleus-nucleus interaction to the *NN* interaction. This can be obtained by folding an effective *NN* interaction over the density distribution of the two nuclei. This model is known as the double folding (DF) model [16]. It has been used widely and has been found to be quite successful in evaluating the α decay half-lives [9,11,12]. The folded nuclear potential is written as

$$V_N(\mathbf{r}) = \int d\mathbf{r}_c d\mathbf{r}_d \, \rho_1(\mathbf{r}_c) v_N(|\mathbf{s}| = |\mathbf{r} + \mathbf{r}_c - \mathbf{r}_d|) \rho_2(\mathbf{r}_d), \tag{4}$$

where ρ_i ($i = 1, 2$) are the densities of the cluster and the daughter nucleus in a decay, and $v_N(|\mathbf{s}|)$ is the nucleon-nucleon (*NN*) interaction. The matter density distribution of the daughter or cluster nucleus can be calculated as

$$\rho(r) = \frac{\rho_0}{1 + \exp\left(\frac{r-R}{a}\right)}, \tag{5}$$

where ρ_0 is obtained by normalizing $\rho(r)$ to the mass number, $\int \rho(\mathbf{r}) \, d\mathbf{r} = A$, and the constants are given as $R = 1.07 A^{1/3}$ fm and $a = 0.54$ fm. If the emitted cluster is an α particle, its matter density distribution is given using a standard Gaussian form [16], namely,

$$\rho_\alpha(r) = 0.4229 \exp(-0.7024 \, r^2). \tag{6}$$

A popular choice of the effective *NN* interaction is based on the M3Y-Reid-type soft core potential,

$$v_N(|\mathbf{s}|) = 7999 \frac{\exp(-4|\mathbf{s}|)}{4|\mathbf{s}|} - 2134 \frac{\exp(-2.5|\mathbf{s}|)}{2.5|\mathbf{s}|}, \tag{7}$$

where $|\mathbf{s}| = |\mathbf{r} + \mathbf{r}_c - \mathbf{r}_d|$ is the distance between a nucleon in the daughter nucleus and a nucleon in the cluster (Fig. 1). This consists of a short-ranged repulsion and a long-ranged attraction responsible for the direct component of the interaction. An additional zero-range contribution $J_{00} \delta(\mathbf{s})$ with $J_{00} = -276(1 - 0.005 \, E/A_c)$ called knock-on exchange term takes into account the antisymmetrization of identical nucleons in the cluster and the daughter nucleus. The latter represents a kind of nonlocality in the DF potential and is usually not included in the calculation if one uses nonlocal nuclear potentials, in order to avoid double counting. Hence, the results in

the present work will also be presented without the inclusion of the knock-on exchange term.

As mentioned above, the nuclear potential is modified, multiplying by a constant λ such that the Bohr-Sommerfeld quantization condition is satisfied:

$$\int_{r_1}^{r_2} k(r)\,dr = \left(n + \frac{1}{2}\right)\pi, \qquad (8)$$

where $k(r) = \sqrt{\frac{2\mu}{\hbar^2}|V(r) - Q|}$ and n is the number of nodes of the quasibound wave function of the cluster nucleus relative motion. This is expressed as $n = (G - l)/2$, where G is a global quantum number and l is the orbital angular momentum quantum number. The calculated optimal value of G for cluster decay is chosen according to the Wildermuth-Tang condition [17,18],

$$G = 2n + l = \sum_{i=1}^{A_c} \left(g_i^{(A_c+A_d)} - g_i^{(A_c)}\right), \qquad (9)$$

where $g_i^{(A_d+A_c)}$ are the oscillator quantum numbers of the nucleons forming the cluster required to ensure that the cluster is completely outside the shell occupied by the daughter nucleus, and $g_i^{(A_c)}$ are the internal quantum numbers of the nucleons in the emitted cluster. The values of g_i are taken as $g_i = 4$ for nucleons in the $50 \leqslant Z$, $N \leqslant 82$ shell, $g_i = 5$ for nucleons in the $82 < Z$, $N \leqslant 126$ shell, $g_i = 6$ for nucleons in the $N \leqslant 184$, and $g_i = 7$ for nucleons outside the $N = 184$ neutron shell closure. These values correspond to the $4\hbar\omega$, $5\hbar\omega$, $6\hbar\omega$, and $7\hbar\omega$ harmonic-oscillator shells, respectively.

The condition in Eq. (9) ensures that the bound state between the light cluster and the heavy daughter nucleus is an allowed state. It gives us the global quantum number, G, that relates the number of nodes, n, to the shell model (in this case within a harmonic oscillator basis) and ensures that the Pauli exclusion principle is satisfied [18]. In other words, it ensures that the α or light cluster is outside the shell occupied by the daughter. This nonlocality is not the same as that included through the exchange term or the nonlocal framework of the present work. We refer the reader to Refs. [19,20] for possible ambiguities introduced by the introduction of this condition in the case of certain kind of potentials.

The Coulomb potential $V_C(r)$ is obtained by using a similar DF procedure with the matter density distributions being replaced by their respective charge density distributions, $\rho^C(r)$. The charge density distributions are taken to have a similar form as that of the matter densities but they are normalized to the number of protons, $\int \rho^C(\mathbf{r})\,d\mathbf{r} = Z$. The fundamental interaction is the standard proton-proton Coulomb interaction $v_C(\mathbf{s}) = \frac{e^2}{|\mathbf{s}|}$. For both nuclear and Coulomb potentials, six-dimensional integrals are involved. These are solved numerically by working in momentum space. The detailed procedure can be found in Ref. [16].

B. Nonlocality

The existence of nonlocal interactions is a purely quantum mechanical phenomenon. This phenomenon arises because of the very nature of nucleons. When calculating an interaction

potential between nuclei, a nonlocality effect appears. This kind of effect has often been discussed in literature in the context of nucleon-nucleus scattering [21–23]. Taking into account nonlocal approaches improves the description of nuclear interactions; however, introducing nonlocality results in an integrodifferential Schrödinger equation which can be, in principle, quite difficult to solve. The general form of this equation is written as

$$-\frac{\hbar^2}{2\mu}\nabla^2 \Psi(\mathbf{r}) + [V_L(\mathbf{r}) - E]\Psi(\mathbf{r})$$

$$= -\int d\mathbf{r}'\, V_{\mathrm{NL}}(\mathbf{r}, \mathbf{r}')\Psi(\mathbf{r}'), \qquad (10)$$

where V_L can be some isolated local potential and V_{NL} can be the nonlocal one.

The sources of nonlocalities in literature are globally classified into two types: the Feshbach and the Pauli nonlocalities [24]. The Feshbach nonlocality is attributed to inelastic intermediate transitions in scattering processes. In other words, the description of an excitation at a point $\mathbf{r}$ in space followed by an intermediate state which propagates and de-excites at some point $\mathbf{r}'$ to get back to the elastic channel (virtual excitations) is contained in the right-hand side of Eq. (10). In this work, we shall not consider the Feshbach nonlocality. The Pauli nonlocality is attributed to the exchange effects which require antisymmetrization of the wave function between the projectile and the target.

In order to solve Eq. (10), it is necessary to know the explicit form of $V_{\mathrm{NL}}(\mathbf{r}, \mathbf{r}')$, which as such is not known. However, we do know that V_{NL} should be such, that in the limit of vanishing nonlocality (represented by a nonlocality parameter b, with $b \to 0$), the integrodifferential Schrödinger equation reduces to the homogeneous one. Assuming this, a nonlocal kernel is usually described in literature [25–27] in terms of a factorized form of the potential. The latter is then used to obtain an effective (local) potential which can be used in the homogeneous Schrödinger equation.

In this article, we use two nonlocality models to construct the effective local potential and study the effects of the nonlocality in the α and cluster decay of some heavy nuclei which can decay by both modes. The first approach we consider in which nonlocality is included was proposed by Perey and Buck in the early 1960s [25]. In the Perey-Buck (PB) model, an energy-independent nonlocal potential for elastic neutron-nucleus scattering is suggested in order to study how far the energy dependence of phenomenological local potentials which had been used earlier could be accounted for by nonlocality. To facilitate calculations, the authors assumed that the nonlocal kernel can be written using a separable form with a local potential times a Gaussian part which contains the nonlocality

$$V_{\mathrm{NL}}(\mathbf{r}, \mathbf{r}') = \frac{1}{\pi^{3/2} b^3} U_N\left(\frac{1}{2}|\mathbf{r} + \mathbf{r}'|\right) \exp\left[-\left(\frac{\mathbf{r} - \mathbf{r}'}{b}\right)^2\right],$$

$$\qquad (11)$$

where b is the nonlocality range parameter and U_N is the energy-independent potential. The nonlocality range

parameter in the case of nucleus-nucleus scattering can be expressed as $b = b_0 m_0/\mu$, where b_0 is the nonlocal range of the nucleon-nucleus interaction, m_0 is the nucleon mass, and μ is the α-daughter or cluster-daughter reduced mass [28]. For our calculations, we choose $b_0 = 0.85$ fm. By using the factorized form of Eq. (11), the nonlocal Schrödinger equation is given as

$$\left[\frac{\hbar^2}{2\mu}\nabla^2 + E\right]\Psi_N(\mathbf{r}) = \frac{1}{\pi^{3/2}b^3}\int U_N\left(\frac{1}{2}|\mathbf{r} + \mathbf{r'}|\right)$$
$$\times \exp\left[-\left(\frac{\mathbf{r} - \mathbf{r'}}{b}\right)^2\right]d\mathbf{r'}. \quad (12)$$

By assuming that the nonlocal and local wave functions are approximately the same [$\Psi_N(\mathbf{r}) \approx \Psi_L(\mathbf{r})$], and the potential inside the nucleus is constant, the authors finally obtained a local equivalent potential given by

$$U^{PB}(r)\exp\left\{\frac{\mu b^2}{2\hbar^2}[E - U^{PB}(r)]\right\} = U_N(r). \quad (13)$$

The r dependence in the equation above is introduced by hand and is justified *a posteriori* due to the success of the model in reproducing data. Finally, the transcendental equation [Eq. (13)] is solved to obtain $U^{PB}(r)$. The approximations used by the authors introduce an inconsistency at small r [9], which as we will see later leads to differences in the results between the two nonlocality models we use.

The second approach in which nonlocality is included was developed in Ref. [27]. We will refer to this approach as the Mumbai (M) model. In this approach, the authors use the mean value theorem of integral calculus to solve the integrodifferential Eq. (10). Performing a partial wave expansion of $V_{NL}(\mathbf{r}, \mathbf{r'})$ and $\Psi(\mathbf{r'})$ in Eq. (10), they obtained the radial equation, which, in the absence of the spin orbit and Coulomb interaction was given as

$$\frac{h^2}{2\mu}\left(\frac{d^2}{dr^2} - \frac{l(l+1)}{r^2}\right)u_l(r) + Eu_l(r)$$
$$= \int_0^\infty g_l(r, r')u_l(r')\,dr', \quad (14)$$

where

$$g_l(r, r') = \left(\frac{2rr'}{\sqrt{\pi}b^3}\right)\exp\left(-\frac{r^2 + r'^2}{b^2}\right)$$
$$\times \int_{-1}^1 U_N\left(\frac{|\mathbf{r} + \mathbf{r'}|}{2}\right)\exp\left(\frac{2rr'x}{b^2}\right)P_l(x)\,dx. \quad (15)$$

By making use of the mean value theorem to rewrite the integral on the right-hand side of Eq. (14), and after some simplifications, the authors obtained the homogenized form of the Schrödinger equation,

$$\left[\frac{d^2}{dr^2} - \frac{l(l+1)}{r^2} + \frac{2\mu}{\hbar^2}\left(E - U_l^M(r)\right)\right]u_l(r) = 0, \quad (16)$$

with an effective strong potential given by [27]

$$U_l^M(r) = \int_0^{r_m} g_l(r, r')\,dr', \quad (17)$$

where $g_l(r, r')$ is written as in Eq. (15). The upper limit of the integration over $g_l(r, r')$ is numerically chosen to be the distance at which the integral becomes negligible, which in our case is essentially the range of the nuclear interaction. In contrast to the PB model, the effective potential obtained in the Mumbai approach is energy independent. However, it is dependent on the angular momentum quantum number, l. As a result of these two differences, it shows a different behavior at small distances with $U_l^M \rightarrow 0$ for $r \rightarrow 0$. We refer the reader to Ref. [9] for a detailed discussion of the above differences in the PB and M models. Here we show a comparison of the DF potential $V_N(r)$ and the effective potentials in Figs. 2 and 3. To find the PB local equivalent potential $U^{PB}(r)$, we replace $U_N(r)$ with $V_N(r)$ and use Eq. (13). The local effective Mumbai potential [$U_l^M(r)$] is found using Eq. (17) by doing a similar replacement; namely, U_N in Eq. (15) is replaced by $V_N(r)$. We choose different isotopes of the same nucleus, uranium (U), for comparison in order to see the effect of the l dependence in the potentials. As expected, the behavior of the M and PB potentials is quite different at small distances. Due to the approximation used in the PB model, the potential appears to be almost the same for the different decays and is insensitive to the change in the l value. This pattern is more evident in α decay than in cluster decay.

A few comments regarding the inclusion of antisymmetrization and medium effects within a nonlocal framework are in order here. The authors in Refs. [29,30] have studied the cluster and α decays of several nuclei within a formalism which includes the antisymmetrization through the finite-range exchange part of the nucleon-nucleon interaction [31]. The folding potential in this case becomes energy dependent and becomes nonlocal through the exchange term. The equivalent local potential is obtained by using a localized approximation for the nonlocal densities of the interacting nuclei. One can also include the density dependence of the NN interaction within such a model [32]. As mentioned earlier, in the present work, including antisymmetrization which leads to the so-called "knock-on exchange" term in the M3Y NN interaction will result in double counting. The effective nonlocal potentials used in this work include the exchange term and medium effects of the NN interaction in a phenomenological way through the nonlocality parameter. In Ref. [33], the authors provided a good description of the nucleus-nucleus scattering data with the São Paulo potential (which is similar in spirit to the PB potential) *without* the exchange term or density dependence included in the NN interaction. The authors noted explicitly that including these effects amounts to double counting of the nonlocality effects and does not provide a good description of data. The nonlocality parameter defined earlier, namely, $b = b_0 m_0/\mu$, where b_0 is the nonlocal range of the nucleon-nucleus interaction, m_0 is the nucleon mass, and μ is the α-daughter or cluster-daughter reduced mass, takes the antisymmetrization and medium effects into account in a phenomenological way.

Finally, we discuss one of the first attempts to evaluate the effects of nonlocality in α decay by Chaudhury [34,35]. The author considered an interaction potential consisting of the pointlike Coulomb interaction between the α and the
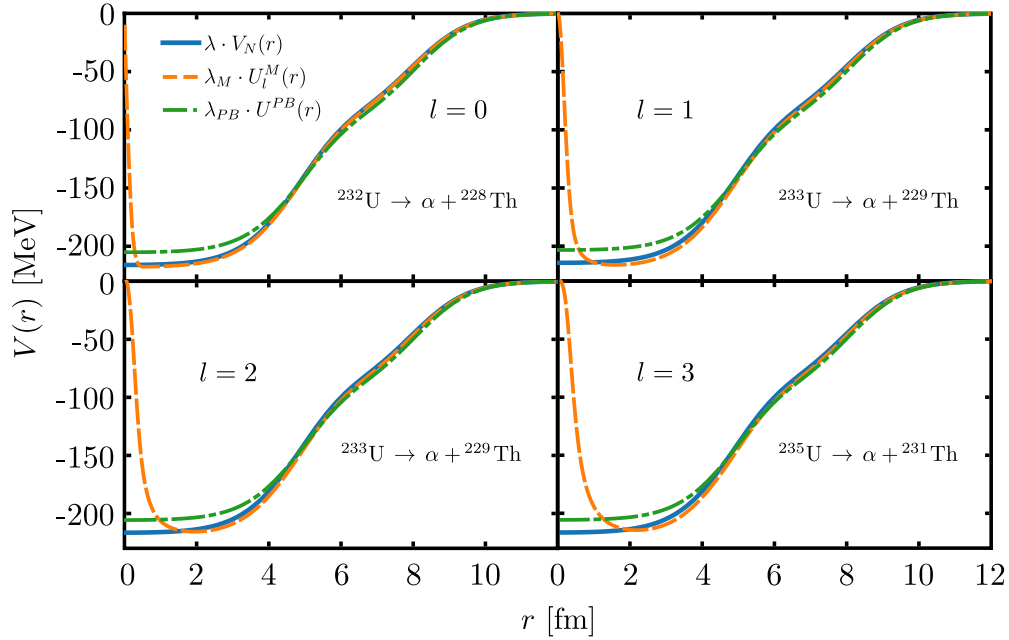
FIG. 2. The nuclear interaction potential between ^{4}He and different isotopes of thorium (Th) in the α decay of the uranium (U) isotopes. The boxes show a comparison of the effective potentials, $U^{\text{PB}}(r)$ (dash-dotted line), $U_l^M(r)$ (dashed line), and the DF potential $V_N(r)$ (solid line) for decays involving different values of the angular momentum quantum number, l.

daughter nucleus superimposed by a nonlocal nuclear potential. The latter was taken to be the Igo potential with the nonlocal part given by a Gaussian function as is used in the approaches mentioned above too. The author obtained a radial differential equation starting from the integrodifferential Eq. (10) with nonlocality and used it to write the JWKB penetration factor. The equation, however, was not the standard radial Schrödinger equation but rather an equation of the form

$$\left[\frac{d^2}{dr^2} - \frac{l(l+1)}{r^2} + \frac{2\mu E\,\epsilon(r)}{\hbar^2} - \frac{2\mu V(r)\,\epsilon(r)}{\hbar^2}\right] u_l(r) = 0,$$

(18)

where the factor $\epsilon(r)$ contained the nonlocality parameter b. The standard JWKB penetration factor is derived by starting
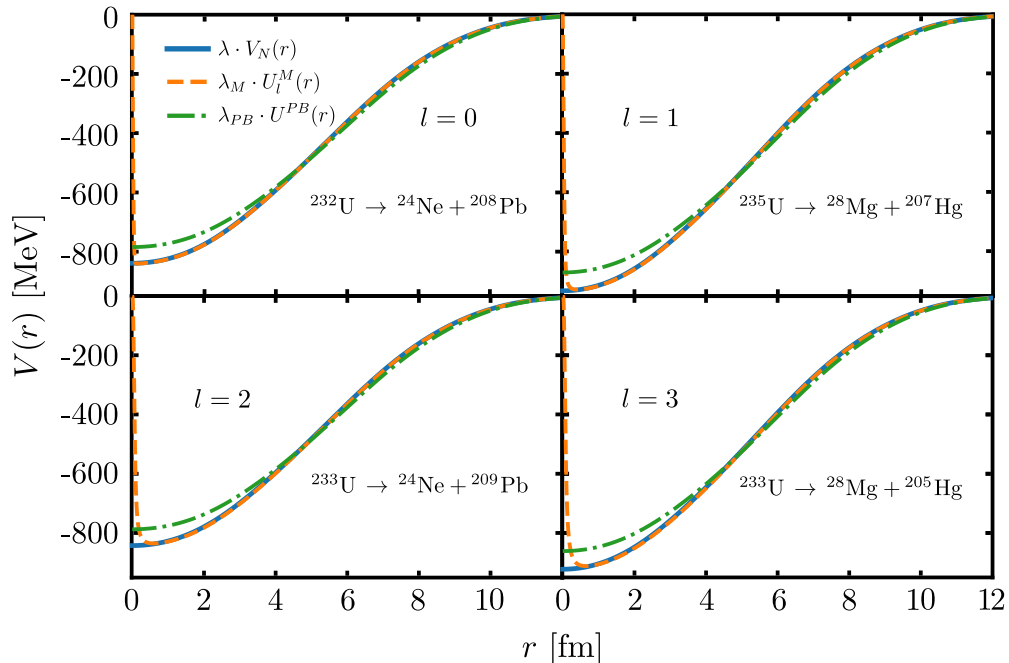
FIG. 3. Same as Fig. 2 but for the different cluster decay modes of the uranium (U) isotopes.

from the radial Schrödinger equation for a particle with energy E, tunneling a potential barrier $V(r)$. However, the author mentions using a JWKB solution of the above equation to obtain the following preformation factor:

$$P = \exp\left\{ -2\sqrt{\frac{2\mu}{\hbar^2}} \int_{r_i}^{r_0} \left[\frac{2(Z-2)e^2}{r}\,\epsilon(r) \right.\right.$$
$$\left.\left. - V_0 f(r)\,\epsilon(r) + \frac{\hbar^2}{2\mu}\frac{l(l+1)}{r^2} - E\,\epsilon(r) \right]^{1/2} dr \right\} \quad (19)$$

where $\epsilon(r) = [1 + \eta f(r)]^{-1}$ and $\eta = (\mu b^2/2\hbar^2)V_0$. The strong potential, $V_0 f(r)$ was taken from the Igo potential. The penetrability was found to increase by about 50% due to nonlocality for the nuclei studied.

C. Potentials for deformed nuclei

The cluster decay half-lives are calculated using the expression of the decay width given by Eq. (2) for the case of spherical nuclei. To extend the cluster decay half-life calculations to deformed nuclei, axial symmetry of nuclei is considered [36]. An additional simplification of the problem is done by considering just one of the nuclei to be deformed [37]. The latter simplification seems to be justified for the decays studied in the present work. Since it is reasonable to consider the α (^{4}He nucleus) to be spherical, in the case of α decay the deformation of the heavy daughter nucleus is taken into account. The heavier daughter in the case of cluster decay is often (the doubly magic nucleus) ^{208}Pb or a nucleus close to it. Thus, in case of cluster decay, we take the deformation of the light cluster into account. This implies the tunneling particle is spherical for α decay and deformed for cluster decay.

For the spherical-deformed interacting system, we begin by writing the nuclear potential between the heavy daughter and the light cluster (or α particle) in Eq. (4) with one spherical density, $\rho_1(r)$, and the other density deformed with axial symmetry, $\rho_2(r, \theta)$. The latter is given as

$$\rho_2(r, \theta) = \frac{\rho_0}{1 + \exp\left[\frac{r - R(\theta)}{a(\theta)}\right]}, \quad (20)$$

where the value of ρ_0 is fixed by normalizing the density distribution $\rho(r, \theta)$ and the angle-dependent half-density radius $R(\theta)$ and diffuseness $a(\theta)$ are given by [37–39]

$$R(\theta) = R_0(1 + \beta_2 Y_{20}(\theta) + \beta_4 Y_{40}(\theta)) \quad (21)$$

and

$$a(\theta) = a_\perp(\theta)\sqrt{1 + |\vec{\nabla} R(\theta)|_{r=R(\theta)}|^2}, \quad (22)$$

respectively. In the above expressions, $R_0 = 1.07 A_d^{1/3}$ fm, β_2 and β_4 are quadrupole and hexadecapole deformation parameters of the deformed nucleus, and

$$a_\perp(\theta) = a_0(1 + \beta_2 Y_{20}(\theta) + \beta_4 Y_{40}(\theta)), \quad (23)$$

where a_0 is taken to be 0.54 fm. As mentioned earlier, the potential in coordinate space is evaluated by converting the six-dimensional integral in Eq. (4) to a momentum space integral. For the decay problem under consideration, this reduces to a one-dimensional integral in momentum space
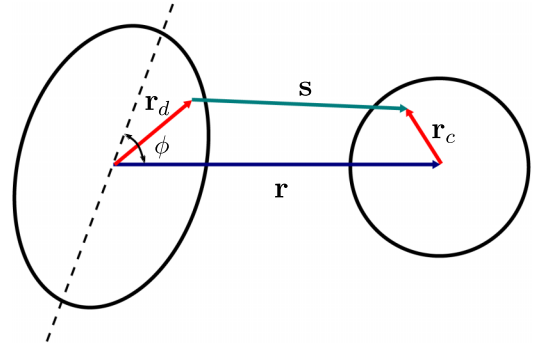
FIG. 4. Schematic representation of the spherical deformed interacting nuclei. ϕ is the orientation angle of the symmetry axis of the deformed nucleus with respect to the vector connecting the center of masses of the two nuclei.

(see Ref. [16] for a detailed derivation with spherical nuclei). When the interacting nuclei are deformed, the shape as well as the orientation of the two nuclei must be taken into account. Assuming one nucleus to be deformed but axially symmetric and the other spherical (for the general case of two deformed nuclei, see Ref. [36]) the DF nuclear potential can be evaluated as a sum of different multipole components [36,40,41]

$$V_N(r, \phi) = \sum_{L=0,2,4\ldots} V_N^L(r, \phi), \quad (24)$$

where ϕ is the orientation angle of the symmetry axis of the deformed nucleus with respect to the vector connecting the center of masses of the two nuclei (Fig. 4). Each of the multipole component is given by the momentum space integral,

$$V_N^L(r, \phi) = \frac{2}{\pi}\left[\frac{2L+1}{4\pi}\right]^{1/2} P_L(\cos\phi)$$
$$\times \int_0^\infty dk\,k^2\,j_L(kr)\rho_1(k)\,\rho_2^L(k)\,v_N(k), \quad (25)$$

such that $\rho_2^L(k)$ is the Fourier transform of

$$\rho_2^L(r) = 2\pi \int \rho_2(r, \theta)\,Y_{L0}(\theta)\,d(\cos\theta). \quad (26)$$

The above is obtained simply from the multipole expansion

$$\rho_2(r, \theta) = \sum_{L=0,2,4} \rho_L(r)Y_{L0}(\theta). \quad (27)$$

The sum in Eqs. (27) and (24) is usually truncated at $L = 4$ to take the dominant form factors into account. The Bohr-Sommerfeld quantization condition, Eq. (8), which is an important constraint for the α and cluster decay half-lives calculations (within the JWKB approximation) and determines the depth of the nuclear potential, is now calculated at each angle. This condition is rewritten as

$$\int_{r_1(\phi)}^{r_2(\phi)} k(r, \phi)\,dr = (G - l + 1)\frac{\pi}{2}, \quad (28)$$

where the turning points are similarly obtained by $V(r_i(\phi), \phi) = Q$. l is the orbital angular momentum quantum

TABLE I. α and cluster decay data. Columns 3 to 6 refer, respectively, to Q value of the decay from the parent ground state (g.s.) to the daughter g.s., the nonlocality parameter, the angular momentum carried by the emitted particle [45,46], and global quantum number given by Eq. (9). The last columns refer to quadrupole β_2 and hexadecapole β_4 deformation parameters of the emitted cluster (c) and daughter nucleus (d), respectively [47,48].

Parent	Decay mode	Q [MeV]	b [fm]	l_{min}	G	$\beta_2^{(c)}$	$\beta_4^{(c)}$	$\beta_2^{(d)}$	$\beta_4^{(d)}$
^{222}Ra	$\alpha + {}^{218}$Rn	6.678	0.2160	0	22	0	0	0.040	0.029
	^{14}C $+ {}^{209}$Pb	33.049	0.0648	0	68	-0.016	0.000	0	0
^{223}Ra	$\alpha + {}^{219}$Rn	5.979	0.2160	2	22	0	0	0.103	0.072
	^{14}C $+ {}^{209}$Pb	31.828	0.0648	4	68	-0.016	0.000	0	0
^{228}Th	$\alpha + {}^{224}$Ra	5.520	0.2160	0	22	0	0	0.164	0.112
	^{20}O $+ {}^{208}$Pb	44.723	0.0466	0	92	0.003	-0.108	0	0
^{231}Pa	$\alpha + {}^{227}$Ac	5.150	0.2160	0	22	0	0	0.172	0.112
	^{23}F $+ {}^{208}$Pb	51.888	0.0411	1	103	-0.202	0.110	0	0
^{232}U	$\alpha + {}^{228}$Th	5.413	0.2160	0	22	0	0	0.182	0.112
	^{24}Ne $+ {}^{208}$Pb	62.310	0.0395	0	106	-0.215	0.155	0	0
^{233}U	$\alpha + {}^{229}$Th	4.908	0.2160	0	22	0	0	0.190	0.114
	^{24}Ne $+ {}^{209}$Pb	60.485	0.0395	2	106	-0.215	0.155	0	0
	^{28}Mg $+ {}^{205}$Hg	74.226	0.0345	3	117	0.323	-0.136	0	0
^{235}U	$\alpha + {}^{231}$Th	4.678	0.2160	1	22	0	0	0.198	0.115
	^{25}Ne $+ {}^{210}$Pb	57.683	0.0381	3	110	0	0	0	0
	^{28}Mg $+ {}^{207}$Hg	72.425	0.0345	1	118	0.323	-0.136	0	0
^{237}Np	$\alpha + {}^{233}$Pa	4.958	0.2160	1	22	0	0	0.207	0.117
	^{30}Mg $+ {}^{207}$Tl	74.790	0.0325	2	127	-0.222	-0.112	0	0
^{236}Pu	$\alpha + {}^{232}$U	5.867	0.2160	0	22	0	0	0.207	0.117
	^{28}Mg $+ {}^{208}$Pb	79.669	0.0345	0	120	0.323	-0.136	0	0
^{241}Am	$\alpha + {}^{237}$Np	5.637	0.2160	1	22	0	0	0.215	0.102
	^{34}Si $+ {}^{207}$Tl	93.926	0.0291	3	141	0	0	0	0
^{242}Cm	$\alpha + {}^{238}$Pu	6.215	0.2160	0	22	0	0	0.215	0.102
	^{34}Si $+ {}^{208}$Pb	96.509	0.0291	0	142	0	0	0	0

number. The global quantum number G is taken to be the same as in the spherical case and is determined by using the Wildermuth-Tang condition, Eq. (9). The deformed Coulomb potential is evaluated in a similar manner by using deformed charge density distributions as in Eq. (20). Thus, the total potential is given by

$$V(r, \phi) = \lambda V_N(r, \phi) + V_C(r, \phi) + \frac{\hbar^2}{2\mu} \frac{\left(l + \frac{1}{2}\right)^2}{r^2}. \quad (29)$$

As a consequence of this orientation angle dependence of the interaction potential, the wave number is also angle dependent, $k(r, \phi)$. Since this term is required to obtain the decay width Γ, it is necessary to average over all possible orientation angles of the deformed nucleus. Some authors average the penetration probability and the normalization factor (or the so-called assault frequency of the tunneling particle related to this) and then multiply them [29,37,41]. However, it is not appropriate since the penetration probability and the normalization factor are not independent of each other. The suitable way to obtain the decay width is then calculating an angle-dependent width,

$$\Gamma(\phi) = \frac{\hbar^2}{2\mu} \left[\int_{r_1(\phi)}^{r_2(\phi)} \frac{dr}{k(r, \phi)} \right]^{-1} \exp\left[-2 \int_{r_2(\phi)}^{r_3(\phi)} k(r, \phi)\, dr \right], \quad (30)$$

and then averaging it over all directions [42–44],

$$\Gamma = \frac{1}{2} \int_0^\pi \Gamma(\phi) \sin\phi \, d\phi. \quad (31)$$

The α and cluster decay half-lives related to the decay width are calculated using Eqs. (1), (30), and (31). The preformation factor is chosen to be 1 and will be determined phenomenologically later.

III. RESULTS AND DISCUSSION

The nonlocal nuclear interaction has been shown to decrease the half-life of spherical nuclei decaying by the emission of α particles [9]. Here we study the combined effects of nonlocality and deformation of the nuclei involved in the decay process. In Table I, Q value of the decay from the parent ground state (g.s.) to the daughter g.s., the nonlocality parameter, the angular momentum carried by the emitted particle [45,46], and global quantum number given by Eq. (9) are listed in columns 3–6. The last columns refer to quadrupole β_2 and hexadecapole β_4 deformation parameters of the emitted cluster (c) and daughter nucleus (d), respectively [47,48].

A. Half-lives

In this section, we shall study the effects of nonlocality and deformation individually as well as their joint manifestation in the α and cluster decay half-lives. The calculations

TABLE II. The calculated α- and cluster-decay half-lives using the DF model (fifth column) and the percentage decrease in the half-lives of different models of nonlocality compared to those evaluated using the DF model without nonlocality. λ, λ_M, and λ_{PB} are the strengths of the nuclear potentials in the DF, M, and PB models.

Parent	Decay mode	$l_{\min}$	Double folding		Mumbai		Perey-Buck	
			λ	$t_{1/2}$ [s]	λ_M	PC	λ_{PB}	PC
^{222}Ra	$\alpha + {}^{218}$Rn	0	2.04	3.28	2.05	3.2	2.32	35.8
	^{14}C + ^{208}Pb	0	1.61	1.10×10^5	1.61	4.1	1.86	76.9
^{223}Ra	$\alpha + {}^{219}$Rn	2	2.04	7.09×10^3	2.10	12.3	2.37	37.0
	^{14}C + ^{209}Pb	4	1.61	3.25×10^7	1.63	17.7	1.86	77.8
^{228}Th	$\alpha + {}^{224}$Ra	0	2.04	8.60×10^6	2.06	3.4	2.37	37.5
	^{20}O + ^{208}Pb	0	1.49	6.78×10^{12}	1.49	3.9	1.72	87.2
^{231}Pa	$\alpha + {}^{227}$Ac	0	2.04	4.30×10^9	2.06	3.2	2.36	38.2
	^{23}F + ^{208}Pb	1	1.43	2.00×10^{14}	1.44	6.4	1.66	90.2
^{232}U	$\alpha + {}^{228}$Th	0	2.04	3.61×10^8	2.05	3.2	2.37	38.2
	^{24}Ne + ^{208}Pb	0	1.42	1.43×10^{10}	1.42	3.8	1.65	91.2
^{233}U	$\alpha + {}^{229}$Th	0	2.04	5.82×10^{11}	2.06	3.3	2.37	38.9
	^{24}Ne + ^{209}Pb	2	1.42	7.25×10^{12}	1.43	10.0	1.65	91.8
	^{28}Mg + ^{205}Hg	3	1.35	5.80×10^{13}	1.36	13.6	1.57	94.6
^{235}U	$\alpha + {}^{231}$Th	1	2.02	3.06×10^{13}	2.07	12.2	2.34	38.9
	^{25}Ne + ^{210}Pb	3	1.41	4.57×10^{17}	1.42	13.6	1.63	92.6
	^{28}Mg + ^{207}Hg	1	1.36	1.10×10^{16}	1.37	6.9	1.58	94.9
^{237}Np	$\alpha + {}^{233}$Pa	1	2.01	1.11×10^{12}	2.06	12.4	2.33	39.2
	^{30}Mg + ^{207}Tl	2	1.35	3.11×10^{14}	1.35	9.6	1.56	94.9
^{236}Pu	$\alpha + {}^{232}$U	0	2.02	9.94×10^6	2.04	3.3	2.35	38.5
	^{28}Mg + ^{208}Pb	0	1.38	1.07×10^9	1.38	3.7	1.60	94.0
^{241}Am	$\alpha + {}^{237}$Np	1	1.99	6.55×10^8	2.04	12.4	2.33	38.9
	^{34}Si + ^{207}Tl	3	1.32	4.33×10^{10}	1.33	12.7	1.54	96.2
^{242}Cm	$\alpha + {}^{238}$Pu	0	1.99	1.28×10^6	2.01	3.4	2.33	39.4
	^{34}Si + ^{208}Pb	0	1.33	9.54×10^8	1.33	3.5	1.55	96.1

are done for two kinds of nonlocal potentials, namely, the energy-independent, so-called Mumbai potential which is l dependent and the well-known Perey-Buck potential which is energy dependent but does not depend on l. We define the percentage change (PC) in the half-life of a nucleus as

$$\text{PC} = \frac{t_{1/2}^{\text{DF}} - t_{1/2}}{t_{1/2}^{\text{DF}}} 100, \qquad (32)$$

where $t_{1/2}^{\text{DF}}$ is the half-life calculated using the DF model only and $t_{1/2}$ is the half-life evaluated within the DF model including nonlocality or deformation or both.

1. Effects of nonlocality

In order to study the change in the half-lives of nuclei due to the nonlocal interaction potential between the decay products, as mentioned before, we use two nonlocal approaches [25,27] from literature which are formally very different. We shall see that though both the approaches are equally successful in reproducing the scattering cross-section data, the manifestation of the nonlocal effects in nuclear decay is quite different within the two approaches. In Table II, the half-lives calculated within the DF model are shown for the α and cluster decay modes of different nuclei. The percentage decrease in the half-life due to the inclusion of nonlocality within the Mumbai and Perey-Buck approach is listed in the next columns. A close look at the numbers reveals the differ-

ences in the two models which are rooted in the nature of the nonlocality model. The main features to be noted from this table are the following:

(i) The percentage decrease [listed as PC and evaluated using Eq. (32)] is much larger in the Perey-Buck approach as compared to the Mumbai model.

(ii) Whereas the PC remains almost constant (around 38% decrease for α decay and around 90% decrease in many cases of cluster decay) within the Perey-Buck approach, this is not the case when the Mumbai model is used.

(iii) Within the Mumbai approach, the percentage decrease in half-life increases significantly with increasing value of the relative angular momentum, l, between the cluster (or α) and the daughter nucleus.

(iv) The decrease in half-lives due to nonlocality is always less in the case of α decay as compared to cluster decay of the same nucleus when the Perey-Buck model is used. Such a pattern does not exist if the nonlocal effects are included within the Mumbai model.

The above features can be understood by noting that (i) whereas the Perey-Buck local equivalent potential, $U^{\text{PB}}(r)$, is derived starting from the full nonlocal Schrödinger equation, the effective Mumbai potential, $U_l^M(r)$, is derived from the *radial* part of the same equation. (ii) As a direct conse-

TABLE III. The calculated α- and cluster-decay half-lives using the DF model (fourth column) and the percentage decrease in the half-lives when different kinds of deformation are included. The fifth column displays the percentage decrease of the half-lives including only the quadrupole deformation parameter β_2 in both $R(\theta)$ and $a_\perp(\theta)$. The sixth column displays the percentage decrease including both the quadrupole and hexadecapole deformation parameters in $R(\theta)$. The diffuseness parameter is constant. The seventh column includes the quadrupole and hexadecapole deformation parameters in both the radius and surface diffuseness parameters.

Parent	Decay mode	l_{min}	$t_{1/2}$ [s] Spherical Double folding	PC		
				Deformed with $R(\theta;\beta_2)$ $a_\perp(\theta;\beta_2)$	Deformed with $R(\theta;\beta_2,\beta_4)$ a_0	Deformed with $R(\theta;\beta_2,\beta_4)$ $a_\perp(\theta;\beta_2,\beta_4)$
^{222}Ra	$\alpha + {}^{218}$Rn	0	3.28	5.9	0.4	8.8
	^{14}C $+ {}^{208}$Pb	0	1.10×10^5	0.4	0.1	0.4
^{223}Ra	$\alpha + {}^{219}$Rn	2	7.09×10^3	8.78	24.8	33.4
	^{14}C $+ {}^{209}$Pb	4	3.25×10^7	0.4	0.1	0.4
^{228}Th	$\alpha + {}^{224}$Ra	0	8.62×10^6	49.1	53.3	66.2
	^{20}O $+ {}^{208}$Pb	0	6.78×10^{12}	0.0	4.3	17.1
^{231}Pa	$\alpha + {}^{227}$Ac	0	4.30×10^9	41.3	57.4	68.2
	^{23}F $+ {}^{208}$Pb	1	2.00×10^{14}	65.7	52.4	78.0
^{232}U	$\alpha + {}^{228}$Th	0	3.63×10^8	46.8	53.9	62.1
	^{24}Ne $+ {}^{208}$Pb	0	1.43×10^{10}	72.0	62.7	87.5
^{233}U	$\alpha + {}^{229}$Th	0	5.82×10^{11}	62.5	48.5	75.4
	^{24}Ne $+ {}^{209}$Pb	2	7.25×10^{12}	72.2	62.9	87.5
	^{28}Mg $+ {}^{205}$Hg	3	5.80×10^{13}	99.5	92.9	98.6
^{235}U	$\alpha + {}^{231}$Th	1	3.06×10^{13}	45.1	66.1	77.9
	^{28}Mg $+ {}^{207}$Hg	1	1.10×10^{16}	99.5	93.1	98.6
^{237}Np	$\alpha + {}^{233}$Pa	1	1.11×10^{12}	51.5	68.8	81.6
	^{30}Mg $+ {}^{207}$Tl	2	3.11×10^{14}	83.7	63.0	80.0
^{236}Pu	$\alpha + {}^{232}$U	0	9.94×10^6	49.3	65.9	76.2
	^{28}Mg $+ {}^{208}$Pb	0	1.07×10^9	99.5	92.7	98.6
^{241}Am	$\alpha + {}^{237}$Np	1	6.55×10^8	54.7	34.5	77.6
^{242}Cm	$\alpha + {}^{238}$Pu	0	1.28×10^6	51.9	62.8	81.2

quence of (i), the Mumbai potential becomes l dependent [see Eqs. (15) and (17)]. (iii) As a consequence of starting with the three-dimensional Schrödinger equation and approximating the nonlocal wave function by the local one, the Perey-Buck potential becomes energy dependent [see Eq. (13)]. (iv) Finally, it must be noted that the derivation of U^{PB} is done under the assumption of a constant potential and the r dependence is introduced *a posteriori*. The latter gives rise to the biggest difference between the two nonlocal potentials; namely, the Mumbai potential vanishes near the origin whereas the Perey-Buck potential attains a large constant value.

In Table II, we also list the values of λ which decide the strength of the nuclear interaction and are obtained by imposing the Bohr-Sommerfeld condition, Eq. (8). They remain roughly the same for the decay processes that have the same emitted cluster and do not display any strong l dependence.

2. Role of deformation

The decay products in the α and cluster decays considered in the present work are not necessarily spherical nuclei. In the case of α decay, it is the daughter nucleus which can be deformed whereas in case of the cluster decay, it is mostly the light cluster which is deformed. The heavier daughter in this latter case is mostly spherical. The nuclear deformation is incorporated through a modification of the interaction po-

tential as described in Sec. II C. In the previous table, we noticed that for a given parent nucleus and within a given approach for nonlocality, the manifestation of the nonlocal effects in the half-life of the nucleus depends on the mode of decay (α or cluster). In the same spirit, we could also ask if a deformed interaction potential would affect the half-lives of the same parent nucleus decaying by α or cluster decay, in a different way. In a semiclassical scheme as that of the present work, the decay is described by the tunneling of the lighter decay product through the Coulomb barrier created by the interaction between the decay products. Seeing it from this point of view, in the case of α decay, the tunneling nucleus is spherical (and the heavy daughter deformed), whereas in case of cluster decay, it is the deformed light nucleus which tunnels through the barrier generated due to its interaction with the spherical heavier daughter nucleus.

Table III displays the percentage change in the half-lives of various nuclei decaying by the two modes, namely, α and cluster decay. The last column lists the results with a complete inclusion of the deformation effects in the radius as well as diffuseness parameter in the potential. The fifth and the sixth columns show the effect of ignoring some of the terms involving the hexadecapole and quadrupole deformation (these columns are listed for completeness since such omissions are sometimes found in literature). In spite of the tunneling picture considered above, deformation manifests itself in a similar way in both α and cluster decay.

TABLE IV. The calculated α- and cluster-decay half-lives using the DF model and the percentage decrease in half-lives when different models of nonlocality and different kinds of deformation are included. The last two columns represent the complete calculation with β_2 and β_4 included in the radius and surface diffuseness parameters. Other columns show the effect of dropping one or both deformation parameters for each model of nonlocality.

Parent	Decay mode	l_{min}	$t_{1/2}$ [s] Spherical double folding	PC Deformed with $R(\theta;\beta_2)$ and $a_\perp(\theta;\beta_2)$		Deformed with $R(\theta;\beta_2,\beta_4)$ and a_0		Deformed with $R(\theta;\beta_2,\beta_4)$ and $a_\perp(\theta;\beta_2,\beta_4)$	
				Mumbai	Perey-Buck	Mumbai	Perey-Buck	Mumbai	Perey-Buck
^{222}Ra	α + ^{218}Rn	0	3.28	9.1	39.6	4.2	35.9	12.3	40.8
	^{14}C + ^{209}Pb	0	1.10×10^5	4.4	77.0	4.2	76.9	4.4	77.0
^{223}Ra	α + ^{219}Rn	2	7.09×10^3	28.4	42.2	33.2	52.3	40.8	57.5
	^{14}C + ^{209}Pb	4	3.25×10^7	18.0	77.9	17.8	77.9	18.0	77.9
^{228}Th	α + ^{224}Ra	0	8.62×10^6	50.3	68.0	54.2	70.8	67.3	79.8
	^{20}O + ^{208}Pb	0	6.78×10^{12}	3.9	87.2	8.0	87.8	20.4	89.5
^{231}Pa	α + ^{227}Ac	0	4.30×10^9	41.5	64.4	58.8	73.8	69.8	83.4
	^{23}F + ^{208}Pb	1	2.00×10^{14}	68.0	96.8	55.5	95.5	79.4	98.0
^{232}U	α + ^{228}Th	0	3.63×10^8	54.1	65.7	55.5	71.6	63.9	77.0
	^{24}Ne + ^{208}Pb	0	1.43×10^{10}	73.0	97.7	64.2	96.9	88.0	99.0
^{233}U	α + ^{229}Th	0	5.82×10^{11}	63.8	76.9	50.3	67.2	76.8	86.2
	^{24}Ne + ^{209}Pb	2	7.25×10^{12}	75.0	97.8	66.7	97.1	88.8	99.1
	^{28}Mg + ^{205}Hg	3	5.80×10^{13}	99.6	100.0	93.8	99.6	98.8	99.9
^{235}U	α + ^{231}Th	1	3.06×10^{13}	62.7	64.5	70.3	80.5	78.3	86.9
	^{25}Ne + ^{210}Pb	3	4.57×10^{17}	13.6	92.6	13.6	92.6	13.6	92.6
	^{28}Mg + ^{207}Hg	1	1.10×10^{16}	99.5	100.0	93.6	99.7	98.7	99.9
^{237}Np	α + ^{233}Pa	1	1.11×10^{12}	63.8	67.7	72.5	81.8	82.9	89.3
	^{30}Mg + ^{207}Tl	2	3.11×10^{14}	85.3	99.2	66.5	98.1	81.9	99.0
^{236}Pu	α + ^{232}U	0	9.97×10^6	53.3	69.4	66.9	79.8	77.3	87.2
	^{28}Mg + ^{208}Pb	0	1.07×10^9	99.5	100.0	93.0	99.6	98.6	99.9
^{241}Am	α + ^{237}Np	1	6.55×10^8	55.8	73.5	43.2	61.1	78.5	86.1
	^{34}Si + ^{207}Tl	3	4.33×10^{10}	12.7	96.2	12.7	96.2	12.7	96.2
^{242}Cm	α + ^{238}Pu	0	1.28×10^6	54.9	71.0	65.4	77.8	81.9	87.3
	^{34}Si + ^{208}Pb	0	9.54×10^8	3.5	96.1	3.5	96.1	3.5	96.1

The half-lives decrease after the inclusion of deformation in the interaction potential. The effect is not sensitive to the sign of the deformation parameters but is greater for larger magnitudes of the parameters.

3. Half-lives with a nonlocal and deformed interaction potential

In Table IV, we show the effects of including both non-locality and deformation in the interaction potential between the daughter nuclei. This table is in principle meant to display the overlap of the effects shown in Tables II and III. However, the overlap of the two effects cannot be expected to be linear. Nonlocality and deformation both lead to a decrease in the α as well as cluster decay half-lives. Since the decrease due to nonlocality in the Perey-Buck model is already large, one does not see a significant difference in the results with nonlocality and deformation together. The Mumbai model, however, displayed a smaller decrease in half-lives due to nonlocality and including deformation enhances the effect a lot. The effect is more enhanced for larger values of the angular momentum quantum number l. Once again, this difference between the results using the two different approaches for nonlocality could be due to the fact that whereas the Mumbai potential is l dependent but energy independent, the Perey-Buck potential is energy dependent but not l dependent. It is interesting to note that both potentials can reproduce scattering data equally well. The latter is understandable since the differences in the models would not show up in the calculation of total cross sections (where we sum over all partial waves). In this sense, the α or the cluster decay of a nucleus which picks up a particular l value can be a better handle to distinguish between different models of nonlocality and fine tune them in a better way.

B. Preformation factors

The phenomenon of the emission of ^{4}He (α) and light nuclei such as ^{14}C, ^{20}O, ^{23}F, $^{24-25}$Ne, $^{28-30}$Mg, and ^{34}Si in the radioactive decay of nuclei can be explained quite well within a preformed cluster model where the decaying parent nucleus is a cluster of the two decay products [29,30,49]. The probability of formation of an α particle or a light cluster inside the parent nucleus is proportional to the overlap of the wave function of the final state with that of the initial state. However, one can determine this quantity in a phenomenological way within the preformed cluster model. Within such a model, one usually defines the decay constant or the width as a product of the preformation factor, P_i ($i = \alpha$ or c here), assault

TABLE V. The calculated α- and cluster-decay preformation factor P_i ($i = \alpha$ or c) using the DF model (fourth column), different models of nonlocality (fifth and sixth columns), and including different kinds of deformation (seventh, eighth, and ninth columns). The last column represents the calculation with β_2 and β_4 included in the radius and diffuseness parameters. Since the calculations are performed for transitions from the parent to the daughter ground state (g.s), the branching ratio (B.R.) for the g.s. → g.s. transition, whenever available from experiment is given.

							P_i		
				Spherical				Deformation	
				double	Nonlocality		$R(\theta;\beta_2)$	$R(\theta;\beta_2,\beta_4)$	$R(\theta;\beta_2,\beta_4)$
Parent	Decay mode	B.R.	$l_{\min}$	folding	Mumbai	Perey-Buck	$a_\perp(\theta;\beta_2)$	a_0	$a_\perp(\theta;\beta_2,\beta_4)$
^{222}Ra	$\alpha + {}^{218}$Rn	0.969	0	8.63×10^{-2}	8.35×10^{-2}	5.54×10^{-2}	8.11×10^{-2}	8.59×10^{-2}	7.82×10^{-2}
	^{14}C $+ {}^{208}$Pb	–	0	8.64×10^{-7}	8.29×10^{-7}	2.00×10^{-7}	8.61×10^{-7}	8.63×10^{-7}	8.61×10^{-7}
^{223}Ra	$\alpha + {}^{219}$Rn	0.01	2	7.18×10^{-3}	6.30×10^{-3}	5.42×10^{-3}	6.55×10^{-3}	5.40×10^{-3}	4.82×10^{-3}
	^{14}C $+ {}^{209}$Pb	–	4	2.93×10^{-8}	2.41×10^{-8}	6.50×10^{-9}	2.92×10^{-8}	2.92×10^{-8}	2.92×10^{-8}
^{228}Th	$\alpha + {}^{224}$Ra	0.734	0	1.40×10^{-1}	1.37×10^{-1}	8.37×10^{-2}	7.28×10^{-2}	6.68×10^{-2}	5.23×10^{-2}
	^{20}O $+ {}^{208}$Pb	–	0	1.12×10^{-8}	1.08×10^{-8}	1.44×10^{-9}	1.12×10^{-8}	1.08×10^{-8}	9.31×10^{-9}
^{231}Pa	$\alpha + {}^{227}$Ac	0.110	0	4.16×10^{-3}	4.03×10^{-3}	2.57×10^{-3}	2.44×10^{-3}	1.78×10^{-3}	1.38×10^{-3}
	^{23}F $+ {}^{208}$Pb	–	1	1.91×10^{-12}	1.79×10^{-12}	1.87×10^{-13}	6.56×10^{-13}	9.11×10^{-13}	4.21×10^{-13}
^{232}U	$\alpha + {}^{228}$Th	0.685	0	1.67×10^{-1}	1.61×10^{-1}	1.02×10^{-1}	8.88×10^{-2}	7.69×10^{-2}	6.53×10^{-2}
	^{24}Ne $+ {}^{208}$Pb	–	0	5.91×10^{-11}	1.65×10^{-11}	5.20×10^{-12}	1.48×10^{-10}	2.20×10^{-11}	7.39×10^{-12}
^{233}U	$\alpha + {}^{229}$Th	0.843	0	1.15×10^{-1}	1.12×10^{-1}	7.08×10^{-2}	4.42×10^{-2}	5.95×10^{-2}	3.08×10^{-2}
	^{24}Ne $+ {}^{209}$Pb	–	2	1.04×10^{-12}	9.36×10^{-13}	9.57×10^{-14}	2.89×10^{-13}	1.99×10^{-12}	1.30×10^{-13}
	^{28}Mg $+ {}^{205}$Hg	–	3	1.50×10^{-14}	1.30×10^{-14}	8.12×10^{-16}	7.78×10^{-17}	1.07×10^{-15}	2.12×10^{-16}
^{235}U	$\alpha + {}^{231}$Th	0.0477	1	1.37×10^{-3}	1.21×10^{-3}	8.42×10^{-4}	7.56×10^{-4}	4.67×10^{-4}	3.23×10^{-4}
	^{25}Ne $+ {}^{210}$Pb	–	3	1.65×10^{-10}	1.42×10^{-10}	1.22×10^{-11}	1.65×10^{-10}	1.65×10^{-10}	1.65×10^{-10}
	^{28}Mg $+ {}^{207}$Hg	–	1	3.97×10^{-12}	3.70×10^{-12}	2.03×10^{-13}	1.98×10^{-14}	2.74×10^{-13}	5.41×10^{-14}
^{237}Np	$\alpha + {}^{233}$Pa	0.0239	1	1.64×10^{-2}	1.44×10^{-2}	1.00×10^{-2}	8.00×10^{-3}	5.14×10^{-2}	3.71×10^{-2}
	^{30}Mg $+ {}^{207}$Tl	–	2	1.84×10^{-13}	1.66×10^{-13}	9.37×10^{-15}	2.99×10^{-14}	6.80×10^{-14}	3.68×10^{-14}
^{236}Pu	$\alpha + {}^{232}$U	0.691	0	1.10×10^{-1}	1.06×10^{-1}	6.80×10^{-2}	5.60×10^{-2}	3.77×10^{-2}	2.78×10^{-2}
	^{28}Mg $+ {}^{208}$Pb	–	0	2.38×10^{-13}	2.29×10^{-13}	1.43×10^{-14}	1.17×10^{-15}	1.74×10^{-14}	4.02×10^{-13}
^{241}Am	$\alpha + {}^{237}$Np	0.0037	1	4.80×10^{-2}	4.20×10^{-2}	2.93×10^{-2}	2.22×10^{-2}	3.09×10^{-2}	1.18×10^{-2}
	^{34}Si $+ {}^{207}$Tl	–	3	2.35×10^{-15}	2.05×10^{-15}	8.92×10^{-17}	2.35×10^{-15}	2.35×10^{-15}	2.35×10^{-15}
^{242}Cm	$\alpha + {}^{238}$Pu	0.748	0	9.16×10^{-2}	8.85×10^{-2}	5.52×10^{-2}	4.40×10^{-2}	3.40×10^{-2}	1.88×10^{-2}
	^{34}Si $+ {}^{208}$Pb	–	0	6.78×10^{-15}	6.55×10^{-15}	2.65×10^{-16}	6.78×10^{-15}	6.78×10^{-15}	6.78×10^{-15}

frequency, and the penetration probability. Calculations are performed by setting $P_i = 1$ and the disagreement with the experimental half-life is then attributed to the performation probability. Thus, one evaluates the theoretical width Γ as in Eq. (2), or Eq. (31), with $P_i = 1$, and then defines the probability for cluster formation as [49], $P_i = \Gamma^{\exp}/\Gamma$. Here $\Gamma^{\exp} = \hbar \ln 2/t_{1/2}^{\exp}$ is given by the experimental half-life. Note that in case the parent nucleus decays into more than one channel, one must take the branching ratio for the channel under consideration into account. For decays involving the parents as well as daughter nuclei with nonzero spins, the α or the light cluster can be emitted with a nonzero angular momentum quantum number. In this case, the width calculated using Eq. (2) is in principle a partial width, Γ_l. In order to compare with the experimental (full) width, one would in principle have to consider the sum $\sum_l P_i^{(l)} \Gamma_l = \Gamma^{\exp}$. Indeed, in microscopic calculations, one does consider the so-called "reduced widths" and evaluates the l-dependent preformation factor within a given theoretical model. One of the first such calculations was performed by Mang [50,51] in a test of the shell model with the Po and At isotopes. For a phenomenological determination of the preformation factor

within the preformed cluster model, however, it is customary to define P_i as

$$P_i = \frac{\Gamma^{\exp}}{\Gamma_{l_{\min}}} \qquad (33)$$

with $\Gamma_{l_{\min}}$ evaluated for the minimum l value using Eq. (2) with $P_i = 1$. The above relation is a good approximation if the preformation factors and widths for all $l > l_{\min}$ are much smaller than those for $l_{\min}$. In the absence of any theoretical calculations of P_i confirming the latter, we shall evaluate the preformation factors using Eq. (33), which is commonly found in literature. In the Tables V and VI, we present the effects of nonlocality and deformation on the values of P_i for the different decays discussed earlier. The notation is similar to that used in the tables showing the half-lives and the percentage changes due to nonlocality and deformation. We note that the preformation factors in the tables have been evaluated only for the transitions from the parent ground state (g.s) to the g.s. of the heavy daughter nucleus using Eq. (33). The branching ratio (B.R.) for the transition from (parent) g.s. → (daughter) g.s. is listed in the table in case of α decay and should be multiplied with the values of P_i given in the

TABLE VI. The calculated α- and cluster-decay preformation factor P_i ($i = \alpha$ or c) using the DF model and different models of nonlocality (including deformation partly and fully). The last two columns represent the complete calculation with β_2 and β_4 included in the radius and diffuseness parameters. Other columns show the effect of dropping one or both deformation parameters. B.R. is the branching ratio for the transition from the parent ground state to the daughter ground state as in Table V.

| | | | | | P_i | | | | | |
| | | | | Spherical double | Deformed with $R(\theta;\beta_2)$ and $a_\perp(\theta;\beta_2)$ | | Deformed with $R(\theta;\beta_2,\beta_4)$ and a_0 | | Deformed with $R(\theta;\beta_2,\beta_4)$ and $a_\perp(\theta;\beta_2,\beta_4)$ | |
Parent	Decay mode	B.R.	l_{min}	folding	Mumbai	Perey-Buck	Mumbai	Perey-Buck	Mumbai	Perey-Buck
^{222}Ra	$\alpha + {}^{218}$Rn	0.969	0	8.63×10^{-2}	7.84×10^{-2}	5.20×10^{-2}	8.26×10^{-2}	5.52×10^{-2}	7.58×10^{-2}	5.10×10^{-2}
	^{14}C $+ {}^{208}$Pb	–	0	8.64×10^{-7}	8.26×10^{-7}	1.99×10^{-7}	8.28×10^{-7}	2.00×10^{-7}	8.26×10^{-7}	1.99×10^{-7}
^{223}Ra	$\alpha + {}^{219}$Rn	0.01	2	7.18×10^{-3}	5.14×10^{-3}	4.15×10^{-3}	4.80×10^{-3}	3.42×10^{-3}	4.25×10^{-3}	3.05×10^{-3}
	^{14}C $+ {}^{209}$Pb	–	4	2.93×10^{-8}	2.40×10^{-8}	6.46×10^{-9}	2.41×10^{-8}	6.48×10^{-9}	2.40×10^{-8}	6.46×10^{-9}
^{228}Th	$\alpha + {}^{224}$Ra	0.734	0	1.40×10^{-1}	7.21×10^{-2}	4.57×10^{-2}	6.54×10^{-2}	4.61×10^{-2}	4.99×10^{-2}	2.46×10^{-2}
	^{20}O $+ {}^{208}$Pb	–	0	1.12×10^{-8}	1.08×10^{-8}	1.44×10^{-9}	1.03×10^{-8}	1.38×10^{-9}	8.95×10^{-9}	1.19×10^{-9}
^{231}Pa	$\alpha + {}^{227}$Ac	0.110	0	4.16×10^{-3}	2.43×10^{-3}	1.48×10^{-3}	1.71×10^{-3}	1.09×10^{-3}	1.34×10^{-3}	8.30×10^{-4}
	^{23}F $+ {}^{208}$Pb	–	1	1.91×10^{-12}	6.13×10^{-13}	6.18×10^{-14}	8.51×10^{-13}	8.65×10^{-14}	3.93×10^{-13}	3.84×10^{-14}
^{232}U	$\alpha + {}^{228}$Th	0.685	0	1.67×10^{-1}	7.66×10^{-2}	5.73×10^{-2}	7.61×10^{-2}	4.73×10^{-2}	6.31×10^{-2}	4.25×10^{-2}
	^{24}Ne $+ {}^{208}$Pb	–	0	5.91×10^{-11}	1.59×10^{-11}	1.38×10^{-12}	2.12×10^{-11}	1.84×10^{-12}	7.11×10^{-12}	5.86×10^{-13}
^{233}U	$\alpha + {}^{229}$Th	0.843	0	1.15×10^{-1}	5.68×10^{-2}	2.67×10^{-2}	5.76×10^{-2}	3.80×10^{-2}	2.98×10^{-2}	1.81×10^{-2}
	^{24}Ne $+ {}^{209}$Pb	–	2	1.04×10^{-12}	2.60×10^{-13}	2.27×10^{-14}	3.46×10^{-13}	3.03×10^{-14}	1.17×10^{-13}	9.69×10^{-15}
	^{28}Mg $+ {}^{205}$Hg	–	3	1.50×10^{-14}	6.71×10^{-14}	3.49×10^{-15}	9.29×10^{-16}	5.64×10^{-17}	1.84×10^{-16}	1.08×10^{-17}
^{235}U	$\alpha + {}^{231}$Th	0.0477	1	1.37×10^{-3}	5.14×10^{-4}	4.88×10^{-4}	4.09×10^{-4}	2.67×10^{-4}	2.99×10^{-4}	1.80×10^{-4}
	^{25}Ne $+ {}^{210}$Pb	–	3	1.65×10^{-10}	1.42×10^{-10}	1.22×10^{-11}	1.42×10^{-10}	1.22×10^{-11}	1.42×10^{-10}	1.22×10^{-11}
	^{28}Mg $+ {}^{207}$Hg	–	1	3.97×10^{-12}	1.84×10^{-14}	8.50×10^{-16}	2.56×10^{-13}	1.38×10^{-14}	5.05×10^{-14}	2.63×10^{-15}
^{237}Np	$\alpha + {}^{233}$Pa	0.0239	1	1.64×10^{-2}	5.94×10^{-3}	4.31×10^{-3}	4.52×10^{-3}	3.00×10^{-3}	3.24×10^{-3}	2.09×10^{-3}
	^{30}Mg $+ {}^{207}$Tl	–	2	1.84×10^{-13}	2.70×10^{-14}	1.45×10^{-15}	6.16×10^{-14}	3.46×10^{-15}	3.33×10^{-14}	1.85×10^{-15}
^{236}Pu	$\alpha + {}^{232}$U	0.691	0	1.10×10^{-1}	6.27×10^{-2}	3.38×10^{-2}	3.65×10^{-2}	2.28×10^{-2}	2.62×10^{-2}	1.56×10^{-2}
	^{28}Mg $+ {}^{208}$Pb	–	0	2.38×10^{-13}	1.13×10^{-15}	5.94×10^{-17}	1.67×10^{-14}	1.03×10^{-15}	3.88×10^{-13}	2.81×10^{-14}
^{241}Am	$\alpha + {}^{237}$Np	0.0037	1	4.80×10^{-2}	2.24×10^{-2}	1.27×10^{-2}	2.69×10^{-2}	1.86×10^{-2}	1.03×10^{-2}	6.65×10^{-3}
	^{34}Si $+ {}^{207}$Tl	–	3	2.35×10^{-15}	2.05×10^{-15}	8.92×10^{-17}	2.05×10^{-15}	8.92×10^{-17}	2.05×10^{-15}	8.92×10^{-17}
^{242}Cm	$\alpha + {}^{238}$Pu	0.748	0	9.16×10^{-2}	3.90×10^{-2}	2.64×10^{-2}	3.16×10^{-2}	2.03×10^{-2}	2.27×10^{-2}	1.37×10^{-2}
	^{34}Si $+ {}^{208}$Pb	–	0	6.78×10^{-15}	6.55×10^{-15}	2.65×10^{-16}	6.55×10^{-15}	2.65×10^{-16}	6.55×10^{-15}	2.65×10^{-16}

table in order to determine the performation probability for this particular transition. Thus, the preformation factors for transitions from the parent g.s. to the different excited states of the daughter will differ depending on the B.R. to that level. Since the focus of the present work is to investigate the effects of nonlocality and deformation, we leave such an investigation of g.s. to excited states transitions for the future.

Though the tables give all details of the dependence of the preformation factors on deformation and nonlocality (individually as well as the combined effect), in Fig. 5, we plot the values of P_i for α and cluster decay as a function of the Q values in order to visualize these effects. The two panels show the calculations with two different models of nonlocality with the inclusion of deformation with all the relevant terms in the radius and the diffuseness parameters. The insets show a magnified view of the preformation factors, P_i (with $i = \alpha$) for α decay which appear in the left corner of each panel. Different interesting features emerge from this figure:

(i) All values of P_i evaluated for different isotopes seem to lie on a band, displaying a linear dependence as a function of energy.

(ii) For a given energy, the preformation factors decrease as a function of l (shown by the colored symbols).

(iii) The effect of nonlocality + deformation is more pronounced in case of the Perey-Buck (PB) model (right panel) as compared to the Mumbai model (left panel). The black symbols represent the calculations within the double folding (DF) model without the inclusion of nonlocality or deformation.

The Q values or the energies carried by the α or light cluster are related to the binding energies of the parent and daughter nuclei which in turn also define the formation energy of a cluster [52]. A bigger binding energy of the daughter therefore implies a higher Q value and more internal energy available for the two nuclei in the cluster. The latter explains the decrease in the values of P_i with increasing values of Q. The observation of a linear dependence of the phenomenologically evaluated P_i in Fig. 5 can be useful for theoretical investigations of cluster formation probabilities.

C. Comparison of penetration probabilities

In the section discussing the different approaches for nonlocality, we mentioned one of the earliest works [34,35] studying the effects of the nonlocal strong interaction in α decay. The author evaluated the penetration probabilities for
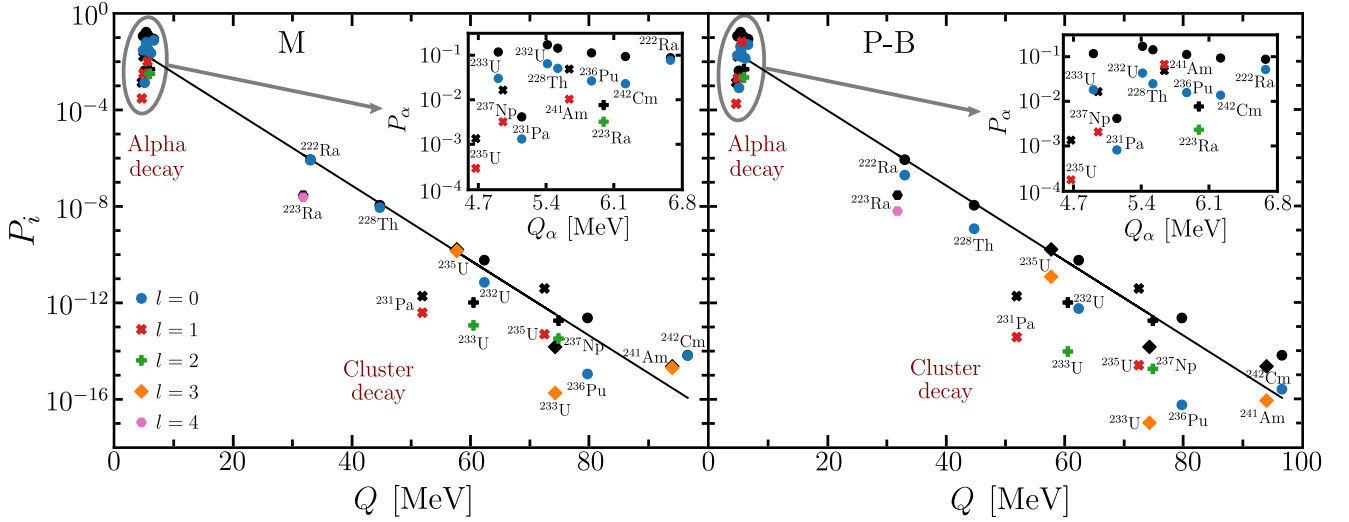
FIG. 5. Preformation factors P_i ($i = \alpha$ or c) as a function of the Q value or energy of the emitted particle in α and cluster decay of different isotopes. The left panel corresponds to the comparison between the DF model (black symbols) and the Mumbai potential including complete deformation (colored symbols representing different values of $l_{\min}$). The right panel compares P_i calculated using the DF and PB models with deformation. The inset shows a magnified view of the α preformation factors which appear to be clubbed together at the small Q values. Most points appear to lie on a band around a straight line which is shown to guide the eye.

the α decay of several nuclei using Eq. (19). In Table VII, we compare the penetration factors obtained in the Mumbai approach studied in this work with that of Ref. [35]. However, in order to perform a consistent comparison, we replace the

Igo potential used in Ref. [35] by the DF one used here and similarly the point-like Coulomb interaction in Eq. (19) is replaced by that obtained using the DF procedure too. Apart from this, recalling that applying the JWKB procedure to the

TABLE VII. Comparison of the penetration probabilities calculated within the Mumbai (M) and Chaudhury (Ch) approach. The effect of nonlocality is expressed in terms of a percentage increase in the penetration factor within the M or Ch model as compared to the double folding model and is given by $PC^{(NL)} = (P^{(NL)} - P^{(DF)}) \times 100/P^{(DF)}$.

Parent	Decay mode	Q [MeV]	$l_{\min}$	$P^{(DF)}$	$PC^{(M)}$	$PC^{(Ch)}$
^{222}Ra	$\alpha + {}^{218}$Rn	6.678	0	7.40×10^{-23}	3.9	7.1
	^{14}C $+ {}^{208}$Pb	33.049	0	3.23×10^{-27}	4.1	7.9
^{223}Ra	$\alpha + {}^{219}$Rn	5.979	2	3.41×10^{-26}	12.2	7.4
	^{14}C $+ {}^{209}$Pb	31.828	4	1.08×10^{-29}	21.1	8.3
^{228}Th	$\alpha + {}^{224}$Ra	5.520	0	2.78×10^{-29}	4.1	5.3
	^{20}O $+ {}^{208}$Pb	44.723	0	5.56×10^{-35}	4.0	10.2
^{231}Pa	$\alpha + {}^{227}$Ac	5.150	0	5.55×10^{-32}	4.2	8.1
	^{23}F $+ {}^{208}$Pb	51.888	1	1.95×10^{-36}	6.8	10.9
^{232}U	$\alpha + {}^{228}$Th	5.413	0	6.60×10^{-31}	4.2	8.1
	^{24}Ne $+ {}^{208}$Pb	62.310	0	2.78×10^{-32}	3.9	10.9
^{233}U	$\alpha + {}^{229}$Th	4.908	0	4.13×10^{-34}	4.1	8.4
	^{24}Ne $+ {}^{209}$Pb	60.485	2	5.41×10^{-35}	11.0	11.7
	^{28}Mg $+ {}^{205}$Hg	74.226	3	7.00×10^{-36}	15.7	13.1
^{235}U	$\alpha + {}^{231}$Th	4.678	1	7.94×10^{-36}	11.8	8.4
	^{25}Ne $+ {}^{210}$Pb	57.683	3	8.57×10^{-40}	15.6	12.5
	^{28}Mg $+ {}^{207}$Hg	72.425	1	3.65×10^{-38}	7.2	13.8
^{237}Np	$\alpha + {}^{233}$Pa	4.958	1	2.19×10^{-34}	11.8	8.0
	^{30}Mg $+ {}^{207}$Tl	74.790	2	1.34×10^{-36}	10.5	12.3
^{236}Pu	$\alpha + {}^{232}$U	5.867	0	2.41×10^{-29}	4.0	8.1
	^{28}Mg $+ {}^{208}$Pb	79.669	0	3.86×10^{-31}	3.8	11.6
^{241}Am	$\alpha + {}^{237}$Np	5.637	1	3.75×10^{-31}	11.9	8.2
	^{34}Si $+ {}^{207}$Tl	93.926	3	1.00×10^{-32}	14.4	12.0
^{242}Cm	$\alpha + {}^{238}$Pu	6.215	0	1.88×10^{-28}	4.1	8.1
	^{34}Si $+ {}^{208}$Pb	96.510	0	4.59×10^{-31}	3.6	11.5

radial equation leads to an improper behavior of the solution near the origin unless one replaces the centrifugal term by the Langer modified term mentioned earlier [15], we replace $l(l+1)$ in Eq. (19) by $(l+1/2)^2$. The Bohr-Sommerfeld quantization, which was not considered in Ref. [35], is also taken into account to obtain a modified version of Eq. (19) given by

$$P^{Ch} = \exp\left\{ -2\sqrt{\frac{2\mu}{\hbar^2}} \int_{r_2}^{r_3} \left[(\lambda V_N(r) + V_C(r) - E) \right. \right.$$

$$\left. \left. \times \epsilon(r) + \frac{\hbar^2(l+1/2)^2}{2\mu r^2} \right]^{1/2} dr \right\} \qquad (34)$$

where V_N is the attractive strong potential whose depth is modified by the factor λ due to the Bohr-Sommerfeld condition. The turning points r_2 and r_3 are given by $V(r) = E$ as before with E taken to be the Q value of the decay.

The penetration factors in both models are found to increase due to the inclusion of nonlocality in the nuclear potential. This is consistent with the fact that the half-lives in general decrease due to nonlocality. The effect is expressed in terms of a percentage change in the penetration probability given by $PC^{(NL)} = (P^{(NL)} - P^{(DF)}) \times 100/P^{(DF)}$. The order of magnitude of the changes are similar in both the models considered. However, the results within the Mumbai approach are sensitive to the l value in the decay. This is expected since the potential defined by Eq. (17), obtained within the Mumbai approach is l dependent.

IV. SUMMARY

In an earlier work [9], the effect of including nonlocality in the nuclear interaction potential was found to decrease the s-wave ($l = 0$) α decay half-lives of spherical nuclei. Results in Ref. [9] indicated that whereas the energy-dependent Perey-Buck (PB) model produced a decrease of 20–40% in the half-lives, $t_{1/2}$, the energy-independent Mumbai (M) potential decreased the half-lives by only 2–4%. Since both the Perey-Buck and Mumbai potentials reproduce the scattering data quite well, this large difference in the decrease of $t_{1/2}$ was surprising. The Mumbai potential is l dependent whereas the Perey-Buck potential does not depend on l. In the calculation of cross sections, where one usually sums over all possible l values to compare with data, the differences between the Mumbai and Perey-Buck potentials do not become quite evident. However, if one considers a nuclear decay, one is actually picking up a particular value of l. Hence, in the present work, different nuclear decays involving nonzero values of l were investigated. Considering nuclei with $l \neq 0$ to be spherical is not always a good approximation. Hence, the above studies were carried out by using a deformed potential whenever necessary. The latter allowed us to also study the effect of deformation on nonlocality.

When a nucleus has the possibility of decaying by emitting an α particle (^{4}He nucleus) or a light cluster (such as ^{14}C, ^{24}Ne, ^{28}Mg, etc.), one can consider the decaying nucleus to be a preformed cluster of an α and a heavy daughter or a light nucleus and a not-so-heavy daughter (^{232}U considered as a preformed cluster of ^{4}He + ^{228}Th or ^{24}Ne + ^{208}Pb, for example). Would the effects of nonlocality (and deformation) show up differently in the two scenarios? To answer this question, the half-lives were calculated for those nuclei which can decay by emitting both an α or a light nucleus. The exercise was rewarding not only in the sense of finding the different manifestation of nonlocality in the two kinds of decays of the same parent nucleus but also in noting the differences in the two nonlocality models studied here.

Since the detailed observations are many, we summarize here the global conclusions drawn from the results:

(i) In the tunneling decay of a nucleus which is considered to be a preformed cluster of the tunneling light nucleus and a heavy daughter, it is important to consider the nonlocality in the interaction potential between the two nuclei forming the cluster.

(ii) Including the effects of deformation of the light nucleus in cluster decay or the heavy daughter in α decay both lead to a decrease in the half-lives of the nuclei. The amount of decrease is decided by the magnitude of the deformation parameters but not affected by the sign of the parameters.

(iii) Sensitivity of the results to the l value (angular momentum) in the decay is manifested within the Mumbai model for nonlocality.

(iv) The combined effect of including deformation and nonlocality (on the half-lives of nuclei) is in general quite large within both models of nonlocality studied here.

(v) Phenomenologically determined cluster preformation factors display a linear dependence on the Q value or the energy carried by the emitted α or light cluster.

Finally, we add that given the nature of the present work with the many ingredients entering into the calculations of half-lives, there is surely scope for better calculations. For example, one could improve the tunneling model by including the intrinsic degrees of freedom of the composite tunneling object as shown in Ref. [53]. Though the nonlocality in the two body interaction has been taken into account, there remains the possibility of including the nonlocality inside the interacting nuclei. Finally, one could replace the semiclassical approach used here by a fully quantum mechanical one or study the nuclear decay within different approaches as in Ref. [43]. Future investigations in this direction can prove useful for a better understanding of nuclear structure as well as nonlocal nuclear interactions.

[1] E. Rutherford, Philos. Mag. **47**, 109 (1899).
[2] D. Ni and Z. Ren, Phys. Rev. C **80**, 051303(R) (2009).
[3] Y. Qian, Z. Ren, and D. Ni, Nucl. Phys. A **866**, 1 (2011).
[4] P. Mohr, Phys. Rev. C **95**, 011302(R) (2017).
[5] W. M. Seif, A. R. Abdulghany, and Z. N. Hussein, J. Phys. G **48**, 025111 (2021).
[6] A. Sandulescu, D. N. Poenaru, and W. Greiner, Sov. J. Part. Nucl. **11**, 528 (1980).
[7] H. J. Rose and G. A. Jones, Nature (London) **307**, 245 (1984).
[8] Y. L. Zhang and Y. Z. Wang, Phys. Rev. C **97**, 014318 (2018).
[9] J. E. Perez Velasquez, N. G. Kelkar, and N. J. Upadhyay, Phys. Rev. C **99**, 024308 (2019).
[10] S. A. Gurvitz and G. Kalbermann, Phys. Rev. Lett. **59**, 262 (1987).
[11] N. G. Kelkar and H. M. Castañeda, Phys. Rev. C **76**, 064605 (2007).
[12] N. G. Kelkar and M. Nowakowski, J. Phys. G: Nucl. Part. Phys. **43**, 105102 (2016).
[13] C. Xu, Z. Ren, G. Röpke, P. Schuck, Y. Funaki, H. Horiuchi, A. Tohsaki, T. Yamada, and B. Zhou, Phys. Rev. C **93**, 011306(R) (2016).
[14] C. Xu, G. Röpke, P. Schuck, Z. Ren, Y. Funaki, H. Horiuchi, A. Tohsaki, T. Yamada, and B. Zhou, Phys. Rev. C **95**, 061306(R) (2017).
[15] R. E. Langer, Phys. Rev. **51**, 669 (1937).
[16] G. Satchler and W. Love, Phys. Rep. **55**, 183 (1979).
[17] K. Wildermuth and Y. C. Tang, *A Unified Theory of the Nucleus* (Springer-Verlag, Berlin, 2013).
[18] D. Ni and Z. Ren, Phys. Rev. C **82**, 024311 (2010).
[19] W. M. Seif, A. M. H. Abdelhady, and A. Adel, Phys. Rev. C **101**, 064305 (2020).
[20] M. Moghaddari Amiri, and O. N. Ghodsi, Phys. Rev. C **102**, 054602 (2020).
[21] A. A. Z. Ahmad, S. Ali, N. Ferdous, and M. Ahmed, Nuov. Cim. A **30**, 385 (1975).
[22] M. A. Cândido Ribeiro, L. C. Chamon, D. Pereira, M. S. Hussein, and D. Galetti, Phys. Rev. Lett. **78**, 3270 (1997).
[23] J. Rotureau, P. Danielewicz, G. Hagen, F. M. Nunes, and T. Papenbrock, Phys. Rev. C **95**, 024315 (2017).
[24] A. B. Balantekin, J. F. Beacom, and M. A. C. Ribeiro, J. Phys. G **24**, 2087 (1998).
[25] F. Perey and B. Buck, Nucl. Phys. **32**, 353 (1962).
[26] L. C. Chamon, B. V. Carlson, L. R. Gasques, D. Pereira, C. De Conti, M. A. G. Alvarez, M. S. Hussein, M. A. Cândido Ribeiro, E. S. Rossi Jr., and C. P. Silva, Braz. J. Phys. **33**, 238 (2003).

[27] N. J. Upadhyay, A. Bhagwat, and B. K. Jain, J. Phys. G **45**, 015106 (2018).
[28] D. Jackson and R. Johnson, Phys. Lett. B **49**, 249 (1974).
[29] A. Adel and T. Alharbi, Nucl. Phys. A **958**, 187 (2017).
[30] A. Adel and T. Alharbi, Braz. J. Phys. **50**, 454 (2020).
[31] D. T. Khoa, Phys. Rev. C **63**, 034007 (2001).
[32] D. T. Khoa, G. R. Satchler, and W. von Oertzen, Phys. Rev. C **56**, 954 (1997).
[33] L. C. Chamon, B. V. Carlson, L. R. Gasques, D. Pereira, C. De Conti, M. A. G. Alvarez, M. S. Hussein, M. A. Cãndido Ribeiro, E. S. Rossi, Jr., and C. P. Silva, Phys. Rev. C **66**, 014610 (2002).
[34] M. L. Chaudhury, Phys. Rev. Lett. **5**, 205 (1960).
[35] M. L. Chaudhury, Phys. Rev. **130**, 2339 (1963).
[36] M. J. Rhoades-Brown, V. E. Oberacker, M. Seiwert, and W. Greiner, Z. Phys. A **310**, 287 (1983).
[37] N. Maroufi, V. Dehghani, and S. Alavi, Nucl. Phys. A **983**, 77 (2019).
[38] A. Bohr and B. Mottelson, *Nuclear Structure: Nuclear Deformations* (W. A. Benjamin, New York, 1969).
[39] G. Scamps, D. Lacroix, G. G. Adamian, and N. V. Antonenko, Phys. Rev. C **88**, 064327 (2013).
[40] M. Ismail, A. Y. Ellithi, and F. Salah, Phys. Rev. C **66**, 017601 (2002).
[41] C. Xu and Z. Ren, Phys. Rev. C **74**, 014304 (2006).
[42] V. Y. Denisov and H. Ikezoe, Phys. Rev. C **72**, 064613 (2005).
[43] D. Ni and Z. Ren, Ann. Phys. **358**, 108 (2015).
[44] Y. Qian, Z. Ren, and D. Ni, Phys. Rev. C **94**, 024315 (2016).
[45] Brookhaven National Laboratory, National Nuclear Data Center, http://www.nndc.bnl.gov.
[46] Institute of Modern Physics, Chinese Academy of Sciences, Atomic Mass Data Center, https://www-nds.iaea.org/amdc/.
[47] P. Moller, J. Nix, W. Myers, and W. Swiatecki, At. Data Nucl. Data Tables **59**, 185 (1995).
[48] G. Sawhney, M. K. Sharma, and R. K. Gupta, Phys. Rev. C **83**, 064610 (2011).
[49] B. B. Singh, S. K. Patra, and R. K. Gupta, Phys. Rev. C **82**, 014607 (2010).
[50] H. J. Mang, Phys. Rev. **119**, 1069 (1960).
[51] H. J. Mang, Z. Phys. **148**, 582 (1957).
[52] D. Deng, Z. Ren, D. Ni, and Y. Qian, J. Phys. G **42**, 075106 (2015).
[53] C. A. Bertulani, V. V. Flambaum, and V. G. Zelevinsky, J. Phys. G **34**, 2289 (2007).